Int. J. Heat Mass Transfer. Vol. 29, No. 12, pp. 1891–1901, 1986
Printed in Great Britain

0017–9310/86 $3.00 + 0.00
Pergamon Journals Ltd.

On the behaviour of a translating vapour bubble under the influence of a pressure step—numerical solutions of implosion and fragmentation

W. M. SLUIJTER, D. G. RODDEMAN and S. J. D. VAN STRALEN
Eindhoven University of Technology, Laboratory for Fluid Dynamics and Heat Transfer, Eindhoven, The Netherlands

(*Received* 30 *October* 1985)

Abstract—The implosion of a translating, originally spherical, free vapour bubble due to a pressure step is described by numerical solution of the basic equations. The treatment is based on the application of a combination of the mathematical methods of collocation and characteristics. The behaviour of a vapour bubble is a generalization of gas bubble behaviour due to the incorporation of the effect of phase transition at the bubble wall. Contrary to a gas bubble, a vapour bubble diminishes completely during the implosion. The theoretical predictions include bubble shape and fragmentation in qualitative agreement with new experimental results.

1. INTRODUCTION

DURING subcooled nucleate boiling, very high heat fluxes can be obtained at a superheated wall. At moderate subcoolings, vapour bubbles depart from the superheated wall, similar to the case of saturated boiling; however, the ascending free vapour bubbles implode due to the subcooling of the bulk liquid. At high subcoolings, bubbles grow and implode simultaneously at the wall.

A subcooling can be created by applying a sudden increase in the ambient pressure to an initially saturated liquid. Immediately after the pressure step, the translating free bubble implodes. The bubble shape will deviate from the original spherical form. In the present paper, the behaviour of an ascending vapour bubble under influence of a sudden pressure step is studied.

Previously, Sluijter *et al.* [1] limited a theoretical treatment to the case of an imploding gas bubble. In that case, the energy equation for the liquid was not taken into account. Growth or implosion of a vapour bubble is very complicated due to the interaction of two mechanisms:

(i) The behaviour of a vapour bubble, hit by a pressure step, differs essentially from that of a gas bubble. Now, condensation or evaporation occur at the bubble boundary during the heat diffusion controlled mode of implosion or growth, respectively. The pressure inside an imploding vapour bubble—which is related thermodynamically to the vapour temperature—is limited, resulting in a complete final bubble implosion.
(ii) For a gas bubble of which the implosion or growth is governed by liquid inertia only, the pressure of the gas follows from the isentropic or isothermal behaviour. In this case, the value of the pressure inside the imploding gas bubble approaches infinity if the volume approaches zero. For this reason, contrary to a vapour bubble, a gas bubble does not implode completely.

Actually, the implosion of a vapour bubble is simultaneously diffusion and inertia controlled; depending on the external conditions, one of these mechanisms dominates during a certain interval.

2. MATHEMATICAL FORMULATION

In principle, a complete set of non-linear equations valid for the case of an incompressible and inviscous liquid can be solved numerically. However, the computing time is then exceptionally long.

For simplicity, a description is given of the behaviour of an imploding free vapour bubble in an infinitely extended, incompressible and inviscous liquid. The compressibility of the vapour is taken into account. The following equations, valid for the liquid surrounding a bubble, are used:

Continuity

$$\nabla . \mathbf{u} = 0. \tag{1}$$

Momentum

$$\frac{\partial \mathbf{u}}{\partial t} = -\frac{1}{\rho}\nabla(p - \mathbf{g}.x) - \mathbf{u}.\nabla\mathbf{u}. \tag{2}$$

Energy

$$\frac{\partial T}{\partial t} = a\nabla^2 T - \mathbf{u}.\nabla T. \tag{3}$$

Equations (1)–(3) and the necessary auxiliary con-

NOMENCLATURE

a liquid thermal diffusivity [$m^2 s^{-1}$]; expansion coefficient in series for liquid velocity in radial direction [$m^{3+k} s^{-1}$]
a_v vapour thermal diffusivity [$m^2 s^{-1}$]
b expansion coefficient in series for liquid velocity in an azimuthal direction [$m^{3+k} s^{-1}$]
c_v specific heat of vapour at constant volume [$J kg^{-1} K^{-1}$]
d initial value of mutual distance between fluid elements in thermal boundary layer around bubble, $\Delta r_j(0)$ [m]
E amount of heat applying to vaporization at the bubble boundary [J]
F_i N-dimensional matrix equation, cf. equation (28)
g gravitational acceleration [$m s^{-2}$]
k liquid thermal conductivity [$W m^{-1} K^{-1}$]
k_v vapour thermal conductivity [$W m^{-1} K^{-1}$]
K_1, K_2, K_3 characteristics
l latent heat of vaporization [$J kg^{-1}$]
m number of sublayers in the liquid layer around bubble
$\mathbf{n}$ unit vector normal to bubble surface
N number of collocation points
p liquid pressure [Pa]
p_v vapour pressure [Pa]
Δp pressure difference, $p_v - p_\infty$ [Pa]
P_k Legendre polynomial of order zero and degree k
Q amount of heat supplied to the bubble [J]
r radial coordinate in spherical coordinate system [m]
R bubble radius, coordinate of bubble wall [m]
R^*, R^{**} principal radii of curvature of a given point at bubble boundary [m]
R_g specific gas constant [$J kg^{-1} K^{-1}$]
R_{eq} equivalent bubble radius, $(3V/4\pi)^{1/3}$ [m]
t time elapsed after start of bubble implosion [s]
Δt time step size at numerical integration [s]
T liquid temperature [K]
T_v vapour temperature [K]
$\mathbf{u}$ liquid velocity vector [$m s^{-1}$]
u_r liquid velocity in r-direction [$m s^{-1}$]
u_ϑ liquid velocity in ϑ-direction [$m s^{-1}$]
u_{tr} translational velocity of bubble [$m s^{-1}$]
U internal energy of vapour in bubble [$J kg^{-1}$]
V volume of vapour bubble [m^3]
W work done by vapour pressure on the surrounding liquid [J]
$\mathbf{x}$ position vector in rectangular coordinates [m].

Greek symbols

δ incremental quantity
Δ difference
ϑ azimuthal angle in spherical coordinates
μ number of successive time steps
ρ liquid density [$kg m^{-3}$]
ρ_v saturated vapour density [$kg m^{-3}$]
σ surface tension coefficient [$kg s^{-2}$].

Other symbols

∇ nabla differential operator [m^{-1}]
∇^2 Laplacian differential operator [m^{-2}].

Subscripts

i integer number denoting collocation point characterized by $R\{\vartheta_i(t)\} = R_i(t)$
j integer number denoting position of fluid element characterized by $r_j(t)$
k integer number in series expansion for liquid velocity
l integer number denoting characteristic point characterized by $R\{\vartheta_l(t)\} = R_l(t)$
v vapour
∞ far away from the bubble.

Superscript

$\dot{}$ first differentiation with respect to time [s^{-1}].

ditions are given expanded in spherical coordinates assuming rotational symmetry, see Fig. 1. A more extensive description of the mathematical treatment is given in ref. [1]. Both the vapour pressure and temperature depend on the rate of heat and mechanical energy supplied to the bubble (Section 4.2).

The following assumptions are made:

(i) Pressure and temperature of the vapour are uniform.
(ii) Thermodynamic equilibrium exist at the bubble boundary, i.e. the vapour temperature equals the liquid temperature: $T = T_v$ at $r = R$.

The liquid pressure at the bubble boundary follows from the Laplace equation:

$$p = p_v - \sigma\left(\frac{1}{R^*} + \frac{1}{R^{**}}\right) \tag{4}$$

which accounts for the discontinuity in the normal stress at the bubble boundary. Conservation of total mass at the moving liquid–vapour interface is expressed by:

$$\rho(\mathbf{u}\,.\,\mathbf{n}) - \rho_v(\mathbf{u}\,.\,\mathbf{n})_v = (\rho - \rho_v)\dot{\mathbf{x}}\,.\,\mathbf{n}. \tag{5}$$

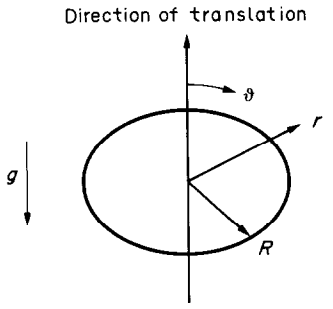

FIG. 1. Bubble with spherical coordinates r, v and R.

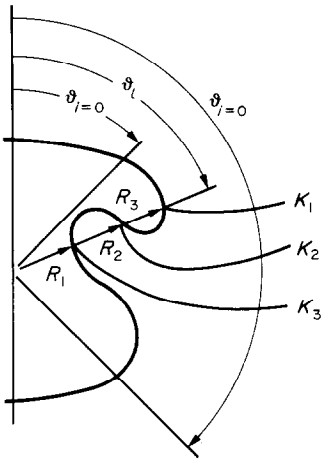

FIG. 2. Two collocation points ($N = 2$) with radius $R_i(t) = R(\vartheta_i, t)$, $i = 0, 1$ and three characteristic points $R_l(t) = R\{\vartheta_l(t)\}$, $\vartheta_{l=1}(t) = \vartheta_{l=2}(t) = \vartheta_{l=3}(t)$, showing a three-valued solution of the bubble radius. K_1, K_2 and K_3 are characteristics.

Equation (5) reduces to:

$$(\mathbf{u}.\mathbf{n}) = \dot{\mathbf{x}}.\mathbf{n} \tag{6}$$

as $\rho_v \ll \rho$, i.e. for operation far below the critical point, and if the contribution of the phase transition to the displacement rate of the bubble boundary is neglected. In view of this, only the equations of motion for the liquid are taken into account.

3. METHOD OF SOLUTION

The bubble shape is described using a combination of the methods of (global, orthogonal) collocation and of characteristics. The collocation method has been applied by Zijl *et al.* [2–4, 6] and by Joosten *et al.* [5]. Sluijter *et al.* [1] applied also the method of characteristics to a translating gas bubble.

3.1. *The collocation method*

The solution of the continuity equation (1) for rotational symmetry without singularities in $\vartheta = 0$ and $r \to \infty$ is given by the following expansion in Legendre polynomials:

$$u_r(r, \vartheta, t) = \sum_{k=0}^{\infty} a_k(t)\left(\frac{1}{r}\right)^{k+2} P_k(\cos\vartheta) \tag{7}$$

$$u_\vartheta(r, \vartheta, t) = \sum_{k=0}^{\infty} b_k(t)\left(\frac{1}{r}\right)^{k+2} P_k(\cos\vartheta). \tag{8}$$

This solution follows from the solution for the velocity potential in an irrotational, incompressible and inviscid liquid flow.

In practice, series (7) and (8) are truncated after N terms. Then the one-dimensional bubble boundary is discretized into N so-called collocation points, each of them representing a fixed (not changing in time) value of ϑ: the collocation angles ϑ_i, $i = O(1)N-1$. The coefficients $a_k(t)$ and $b_k(t)$ are chosen in such a way that at these collocation points the solution of series (7) and (8) satisfies equations (1) and (2). The values of $\cos\vartheta_i$ are chosen as the zeros of a Legendre polynomial, i.e. the convergence to the exact solution for $N \to \infty$ is guaranteed [7].

3.2. *The method of characteristics*

The bubble radius $R_i(t) = R(\vartheta_i, t)$ can also be given by a series expansion which is similar to equations (7) and (8). In that case, a solution of the bubble radius has to be single-valued. However, the method of characteristics allows a multivalued solution for the bubble radius $R_i(t) = R(\vartheta_i, t)$ at a given angle ϑ_i and a fixed time, see Fig. 2.

It is of essential importance that, with the latter method, families of propagation paths of elementary particles are followed adjacent to the moving bubble boundary. In this way, characteristic points are defined which are characterized by $R_l(t) = R\{\vartheta_l(t)\}$, i.e. the characteristic angles $\vartheta_l(t)$ vary in time, contrary to the fixed collocation angles.

The equations for the characteristics are [1]:

$$\frac{d\vartheta}{dt} = \frac{1}{R}u_\vartheta \tag{9}$$

$$\frac{dR}{dt} = u_r. \tag{10}$$

4. THE ENERGY EQUATION

If hit by a pressure step, $\Delta p > 0$, the bubble implodes. During the rapid initial implosion, the vapour behaves as a compressible gas and the compression is adiabatic; both vapour pressure and temperature increase. Immediately afterwards, condensation occurs at the bubble boundary—due to vapour supersaturation—and a thermal boundary layer develops around the bubble. The heat of condensation is removed by conduction in both liquid and vapour adjacent to the bubble boundary (i.e. during advanced implosion, the vapour temperature increases gradually from $T_v = T_v(0)$ to $T_v > T_\infty$).

The thickness of the thermal boundary layer in the liquid increases, and the implosion rate is slowed down; consequently less heat of condensation is liberated. As a result the vapour temperature decreases. Continuation of this process causes oscillations in the decreasing rate of the vapour temperature. The theoretical approach of vapour bubble implosion should involve the hydrodynamic as well as the thermal effect. The latter effect can be split up into that in the liquid and that in the vapour.

4.1. *Liquid*

It is now assumed that the liquid around the bubble is composed by moving fluid elements, each with its own temperature. Consequently, the energy equation has been used as the substantial derivative of the temperature:

$$\frac{\mathrm{d}T}{\mathrm{d}t} = a\nabla^2 T. \tag{11}$$

Actually, the shape of the bubble is not spherical. For simplicity it is assumed that the heat transfer process near the liquid–vapour interface is similar to the case of the equivalent spherical bubble. Consequently, equations (7) and (8) now reduce to:

$$u_\vartheta = 0 \tag{12}$$

$$u_r = \frac{R_{\mathrm{eq}}^2}{r^2}\frac{\delta R_{\mathrm{eq}}}{\delta t}. \tag{13}$$

The liquid adjacent to the bubble boundary is composed of a finite number ($m \geqslant 4$) of successive sublayers, each of them with its own linear temperature gradient, see Fig. 3. The boundaries of the sublayers represent the positions of fluid elements with radii $r_j(t) \geqslant R_{\mathrm{eq}}(t)$ and temperatures $T_j(t)$ to match. Consequently, the heat diffusion equation for the liquid (11) written in rotationally symmetric spherical coordinates becomes:

$$\left(\frac{\mathrm{d}T}{\mathrm{d}t}\right)_j = a\left(\frac{\partial^2 T}{\partial r^2} + \frac{2}{r}\frac{\partial T}{\partial r}\right)_j \tag{14}$$

where

$$\left(\frac{\partial T}{\partial r}\right)_j = \frac{T_{j+1}-T_j}{\Delta r_j} \tag{15}$$

and

$$\left(\frac{\partial^2 T}{\partial r^2}\right)_j = \left\{\frac{(T_{j+2}-T_{j+1})}{\Delta r_{j+1}} - \frac{(T_{j+1}-T_j)}{\Delta r_j}\right\}\Big/\Delta r_j,$$
$$j = 1(1)m-1, \quad m \geqslant 4 \tag{16}$$

with

$$\Delta r_j = r_{j+1} - r_j, \quad j = 1(1)m.$$

The boundary conditions of equation (14) are:

$$T_{j=1} = T\{R_{\mathrm{eq}}(t)\}, \quad T_{j\geqslant m-1} = T_\alpha \tag{17}$$

and the initial conditions:

$$\Delta r_j(0) = d, \quad T_j(0) = T_\infty. \tag{18}$$

According to the second condition of (17) the thermal boundary layer of the bubble consists of $m-2$ sublayers. The outermost two layers in the bulk liquid are needed for the calculations of the second derivative of the temperature at r_{m-2} and r_{m-1}, cf. equation (16). The amount of heat supplied to the bubble, during a small time interval, is given by:

$$\delta Q = 4\pi k R_{\mathrm{eq}}^2 \frac{T_2 - T_1}{\Delta r_1}\delta t \tag{19}$$

where $(T_2-T_1)/\Delta r_1$ is the liquid temperature gradient at the bubble boundary.

4.2. *Vapour*

The total amount of energy transmitted to the vapour in a small time interval is composed of both the thermal energy δQ and the mechanical work done by the vapour pressure on the surrounding liquid:

$$\delta W = \frac{|\dot{R}_{\mathrm{eq}}|}{\dot{R}_{\mathrm{eq}}} p_{\mathrm{v}} 4\pi R_{\mathrm{eq}}^2 \delta R_{\mathrm{eq}} \tag{20}$$

where the vapour pressure p_{v} is assumed to be homogeneous. The energy balance for this liquid–vapour system, i.e. for an open system with phase transition, reads:

$$\delta Q = \delta U + \delta W + \delta E \tag{21}$$

where δQ and δW are given by equations (19) and (20), respectively. In equation (21) is the heat development at the bubble boundary due to phase transition taken into account by:

$$\delta E = l\delta(V\rho_{\mathrm{v}}) \simeq l(V\delta\rho_{\mathrm{v}} + \rho_{\mathrm{v}}\delta V). \tag{22}$$

In general, and in particular at inertia-controlled bubble implosion, $T_{\mathrm{v}} \neq T_{j=1}$. However, in view of the high condensation rate occurring at a free surface, it is assumed that thermodynamic equilibrium exists at the liquid–vapour interface and that $T_{\mathrm{v}} = T_{j=1}$. Also the vapour temperature is assumed to be uniform as $a_{\mathrm{v}} \gg a$. The vapour will be treated as an ideal gas resulting in the equation of state for the energy:

$$\delta U = \rho_{\mathrm{v}} V c_{\mathrm{v}} \delta T_{\mathrm{v}} \tag{23}$$

and for the vapour pressure:

$$p_{\mathrm{v}} = \rho_{\mathrm{v}} R_{\mathrm{g}} T_{\mathrm{v}}. \tag{24}$$

According to equation (24) an expression for a small change in the vapour density, $\rho_{\mathrm{v}} = \rho_{\mathrm{v}}(p, T)$, during a small time interval δt becomes:

$$\delta\rho_{\mathrm{v}} = \frac{\delta p_{\mathrm{v}}}{R_{\mathrm{g}} T_{\mathrm{v}}} - \frac{p_{\mathrm{v}}}{R_{\mathrm{g}} T_{\mathrm{v}}^2}\delta T_{\mathrm{v}}. \tag{25}$$

The relationship between pressure and temperature of the vapour is given by the thermodynamic tables but

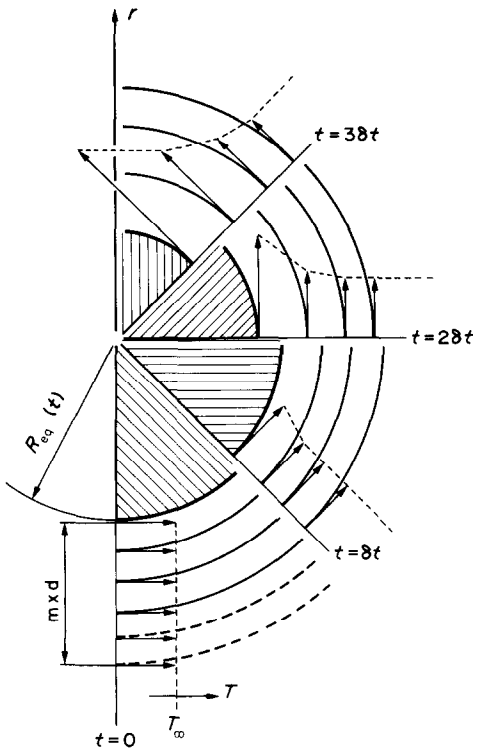

FIG. 3. The evolving of the temperature distribution in the thermal boundary layer around an imploding bubble for $m = 5$ sublayers.

as an approximation of equation (25) the linearized Clapeyron's law is used:

$$\delta p_v = \frac{l p_v}{R_g T_v^2} \delta T_v. \tag{26}$$

Substituting equations (23), (25) and (26) into equation (21) results in an expression for the increase of the vapour temperature during a small time interval δt:

$$\delta T_v = \left(\delta Q - \delta W - \frac{l p_v}{R_g T_v} \delta V\right) \div \left[lV\left(\frac{l p_v}{R_g^2 T_v^3} - \frac{p_v}{R_g T_v^2}\right) + \frac{\rho_v V c_v}{R_g T_v}\right]. \tag{27}$$

Both the vapour pressure and density are determined by the vapour temperature, which, in turn, has been determined by the heat flow rate due to conduction in a thin adjacent liquid layer at the bubble boundary where condensation or evaporation may occur.

Essentially, the condensation heat rate is determined by $\dot{R}$ and, therefore, is principally governed by liquid inertia while the conduction heat rate is determined by the structure of the thermal boundary layer. This structure depends upon the initial region, $m\Delta r_j(0) = md$, around the bubble. Consequently, the choice of the values for m and d influences (theoretically) the implosion behaviour, in addition to the pressure step $\Delta p(0)$, see Section 6.3.

Without change of phase at the bubble boundary one can take $l = 0$ and equation (27) reduces to equation (23).

5. NUMERICAL ANALYSIS

The series of equations (7) and (8) are truncated, see Section 3.1. In that way the following matrix equations are obtained:

$$F_i \begin{Bmatrix} u_r \\ u_\vartheta \end{Bmatrix} = \begin{Bmatrix} u_r(r, \vartheta, t) \\ u_\vartheta(r, \vartheta, t) \end{Bmatrix}_{r = R_i(t)}, \quad i = O(1)N-1. \tag{28}$$

Initially, both the temperature distribution and the flow field in the liquid around the bubble are assumed to be known.

A summary of the numerical procedure which has been used, follows here.

(i) Starting at $t = 0$, the coefficients $a_k(0)$ and $b_k(0)$ are determined by means of equations (28), which are the solutions of equation (1). The initial collocation radii are known from the bubble shape. Now, the liquid velocities at the characteristic points, $R_l(0)$, are calculated from equations (9) and (10) where $\vartheta_l(0) < \vartheta_i(0) < \vartheta_{l+1}(0)$ and $l = 1(1)N+1$.

(ii) After a small time step, Δt, the new characteristic angles and radii are determined by numerical integration of equations (9) and (10). Next, the new collocation radii are determined using an interpolation procedure of the characteristics [1].

(iii) At $t = 0$, both $\partial F_i/\partial r$ and $\partial F_i/\partial t$ are calculated from equations (28) and (2), respectively, which are needed to calculate the values of the liquid velocities on the collocation angles at $t = \Delta t$ by numerical integration of $dF_i/dt = \partial F_i/\partial t + (\partial F_i/\partial r)u_r$, $r = R_i(t)$.

(iv) At $t = \Delta t$, the temperature field of the liquid is determined by integration of equations (14)–(16). The vapour temperature has been calculated using equation (27) with $\delta t = \Delta t$. Subsequently, the vapour pressure is determined by using the thermodynamic tables for equilibrium data.

(v) The new positions of the fluid elements are determined by equations (12) and (13).

Next, the procedure is repeated for each timestep consecutively. The second boundary condition of (17) degenerates into $T_{j \geq \mu+1}(\mu\Delta t) = T_\infty$ for $\mu \leq m-3$, whereas the original condition is relevant for $\mu > m-3$. A single Euler method is used for numerical integration. The calculations have been executed on a Burroughs B7700 computer of the Eindhoven University of Technology.

6. EXPERIMENTAL INVESTIGATIONS

6.1. *Experimental set-up*

As shown in Fig. 4, a stainless-steel vessel is used in the experiments, which contains both a sub-atmospheric liquid section—filled with demineralized water—and a high pressure section—pressurized with nitrogen gas. The sections are separated by a 0.05-mm-thick Mylar sheet and a condenser. The inner dimensions of the liquid section are $115 \times 160 \times 335$ mm (height). This section contains two sets of opposite glass windows to allow high speed motion pictures to be taken with a rotating-prism camera, operating at 4000 f.p.s. Infra-red light, which the quartz windows transmit, is used for liquid heating.

The liquid is preheated to the boiling temperature using a bulk heater. The liquid temperature is then kept constant by means of three infra-red heat sources providing a uniform temperature distribution in the liquid. The static pressure is controlled by a Cartesian manostat. A dynamic pressure transducer is mounted in the bottom plate of the vessel. The observed bubbles are generated at a small thin Ni–Cr wire which is heated by applying an electric current pulse. At the top of the vessel an electromagnetic knife is mounted for the purpose of cutting the Mylar sheet.

6.2. *Experimental method*

The following actions are initiated in chronological order using (adjustable) time delays.

Shortly after the camera is started the Ni–Cr wire is heated at the instant at which the desired motion picture rate is reached. As the generated bubble departs from the wire, the Mylar sheet is cut by forcing the electromagnet with an electric current pulse. This pulse is recorded both on the motion picture by a light emitting diode, mounted appropriately inside the

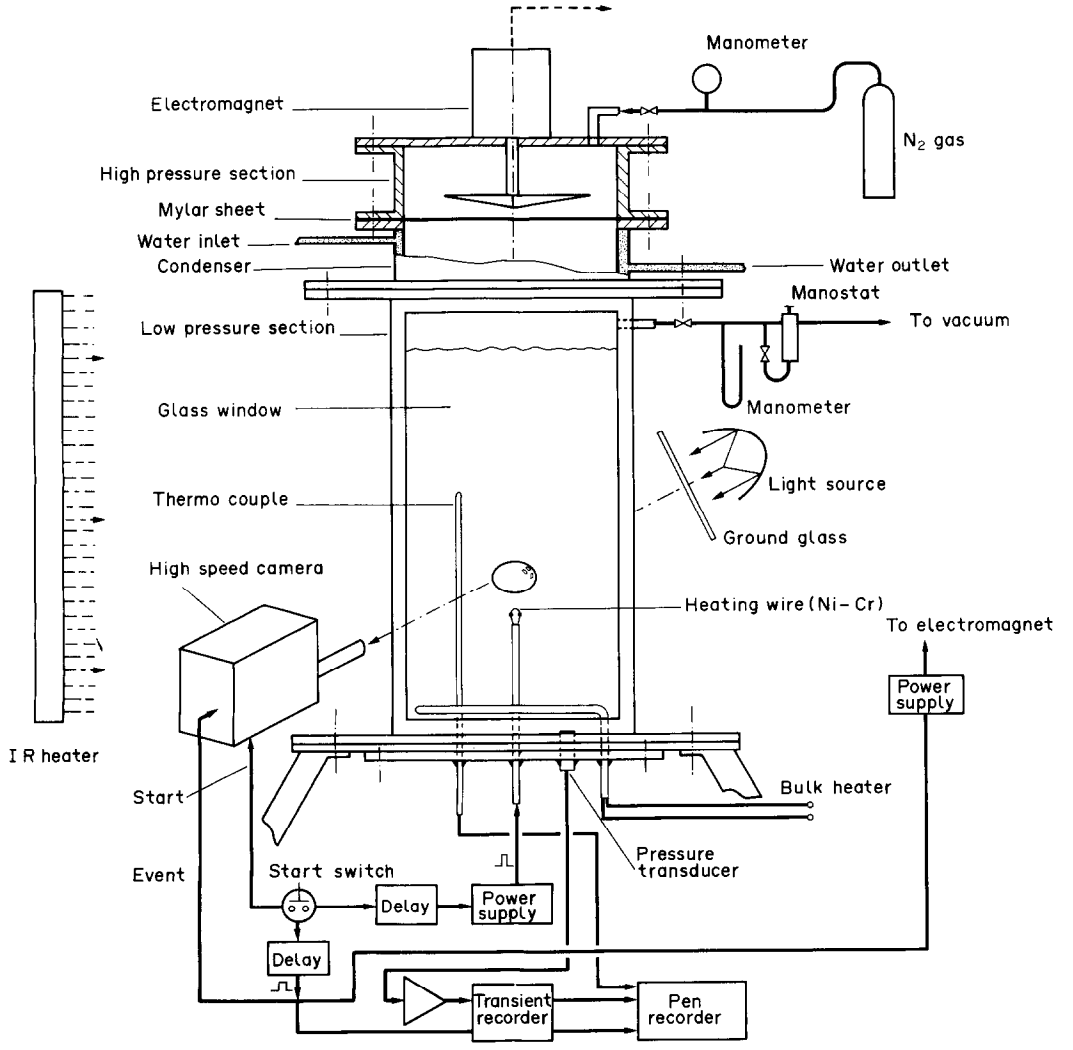

FIG. 4. Diagram of experimental apparatus.

camera, and by a transient recorder for the purpose of synchronizing the recorded data.

Due to the initial high pressure in the pressure section, a pressure wave passes through the low pressure section, where the ascending—nearly spherical—vapour bubble implodes due to the sudden increase on liquid pressure. This increase implies an instant liquid subcooling. During the entire bubble lifetime, the signal of the pressure transducer is recorded—after amplification—on the transient recorder. Figures 5 and 6 show the experimental pressure response, $p_\infty(t)$, of the pressure transducer up to complete implosion of those bubbles which are shown in Figs. 7a and 7b, respectively. The films are analysed frame-by-frame using a motion analyser to obtain quantitative bubble implosion data.

6.3. *Experimental results*

Figures 7a and 7b show photographs of two imploding bubbles—at different initial conditions—taken from a high speed motion picture. At $t = 0$, the bubble is hit by a pressure step, $\Delta p(t) > 0$, and the implosion starts. The accompanying pressure response is represented by the curve drawn in Figs. 5 and 6, respectively. This response deviates from the step function because of both the finite cutting time of the Mylar sheet and the reflection of the pressure wave at the free liquid surface. The dashed curve in Figs. 5 and 6 represents the value of the approximating pressure response, which is used in the calculations. At the time $t = 0$, the bubble is translated over a distance of 0.1 m and the bubble deviates from the original spherical shape as a result of buoyancy. During the implosion (Fig. 7a), the bubble shape of the relatively small bubble changes, but fragmentation does not occur. This is contradictory to the interesting behaviour of a larger bubble (Fig. 7b), which fragments, i.e. a small bubble departs at the rear of the original one.

Figures 8a and 8b show the results of the numerically calculated profile of the bubbles represented in Figs. 7a and 7b, respectively. The origin of the coordinate system has been fixed at the translating bubble centre. In the figures, the origins coincide for the different implosion stages. Because of rotational symmetry the bubble shape at various instants has been drawn for fixed values of ϑ in the interval $[0, \pi]$. The radially directed drawn curves are characteristics, the dashed curves are the collocation angles.

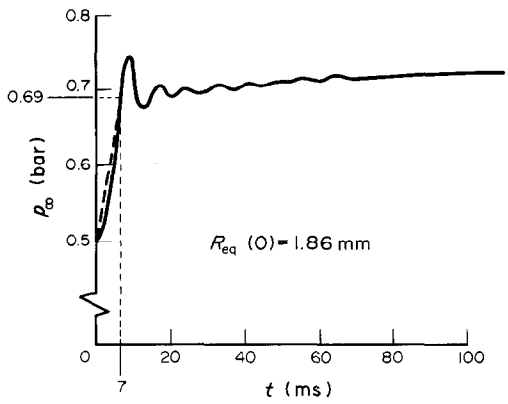

FIG. 5. Pressure response, measured by the pressure transducer for the bubble of Fig. 7a.

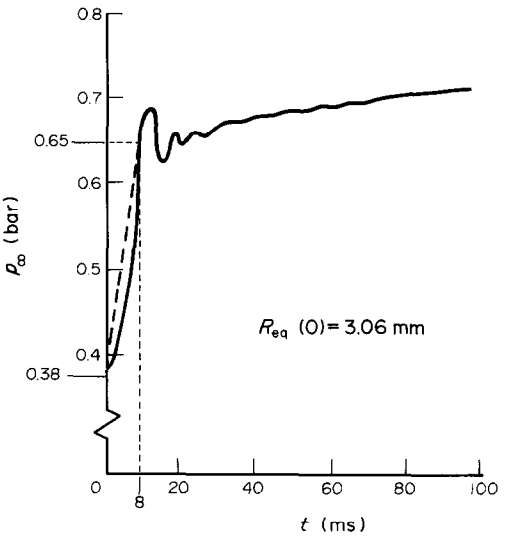

FIG. 6. Pressure response, measured by the pressure transducer for the bubble of Fig. 7b.

The bubble with $R_{eq}(0) = 1.86$ mm shown in Fig. 8a does not fragment within the initial 6 ms, i.e. the bubble is stable. The bubble with $R_{eq}(0) = 3.06$ mm, shown in Fig. 8b, fragments at the axis of rotational symmetry as a toroidal bubble for $t > 1.52$ ms. The latter bubble is unstable, directly after the initial implosion stage, although both bubbles have been hit by a nearly equal pressure step. This tendency is in agreement with the experimental results shown in Figs. 7a and 7b.

Obviously, both the value of m and the initial value of $\Delta r_j(0) = d$ determine the temperature distribution in the thermal boundary layer around the imploding bubble; as a result the implosion rate will be affected, see Section 4.1. Hence, the computations can be fitted to the measured data by choosing the initial temperature field suitable, i.e. by taking appropriate values of m and d.

Figure 9 shows both the experimental data and the computational results for $R_{eq}(t)$ of the bubble shown in Figs. 7a and 8a, respectively. A reasonable fitting of both curves has been achieved for $m = 5$ and $d = 5 \times 10^{-6}$ m; i.e. the initial thickness of the thermal boundary layer amounts to 25×10^{-6} m.

7. CONCLUSIONS

The experimental results show that fragmentation of an imploding vapour bubble occurs under

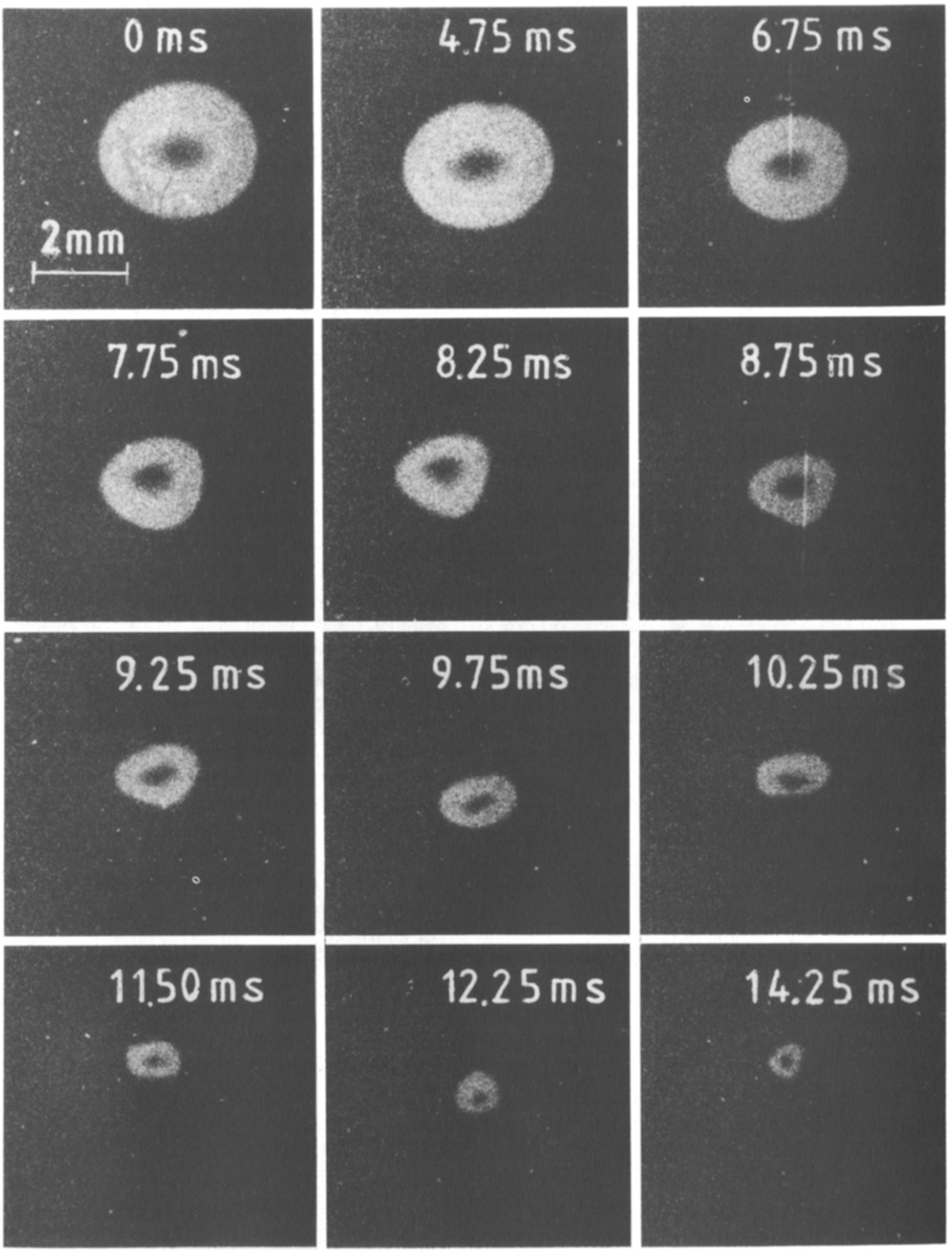

FIG. 7a. Vapour bubble in water, hit by a pressure step $\Delta p(0) = 0.27$ bar (cf. Fig. 5). $T(0) = 354.3$ K, $u_{tr}(0) = 0.23$ m s^{-1}.

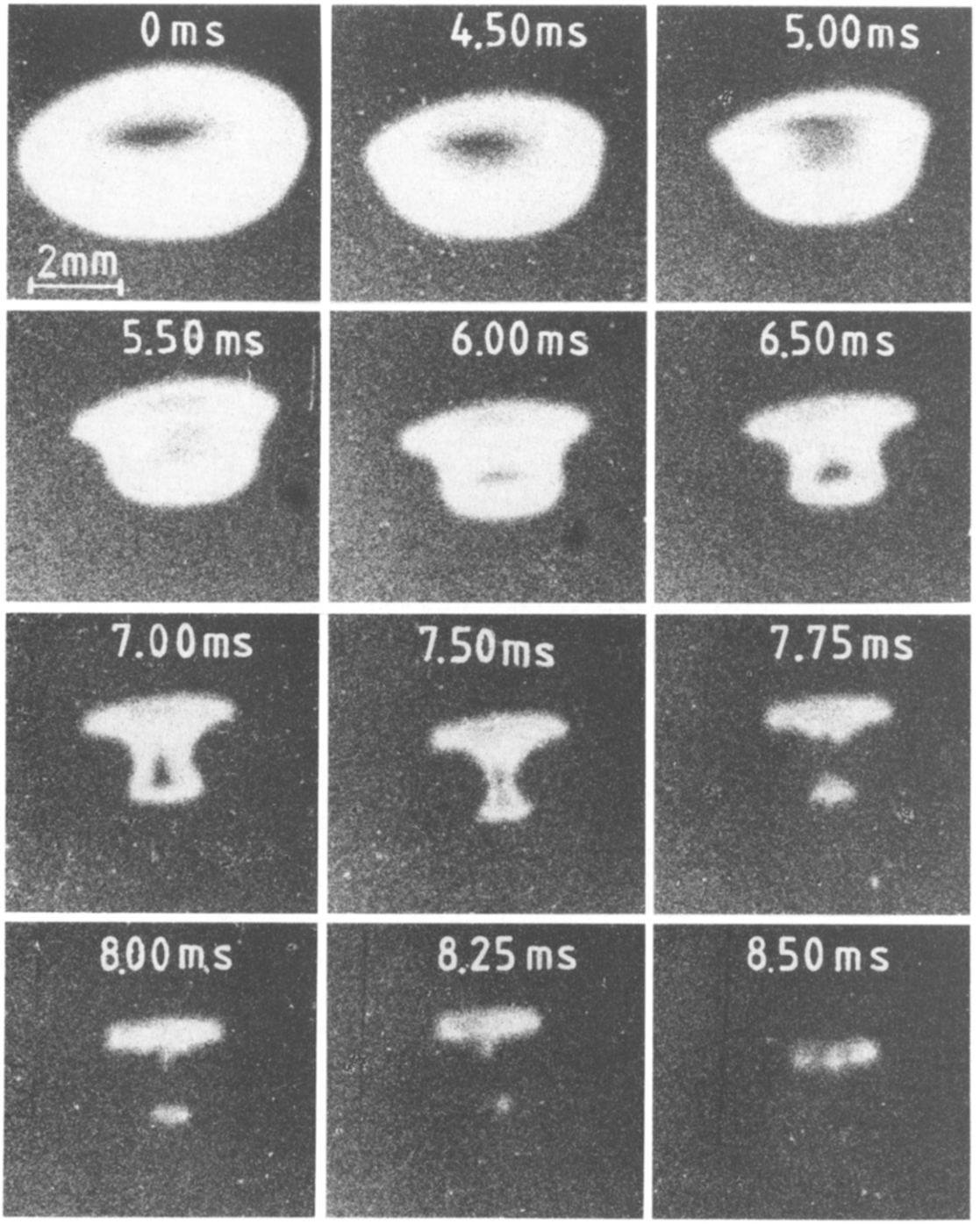

FIG. 7b. Vapour bubble in water, hit by a pressure step $\Delta p(0) = 0.27$ bar (cf. Fig. 6). $T(0) = 347.6$ K, $u_{tr}(0) = 0.2$ m s^{-1}.

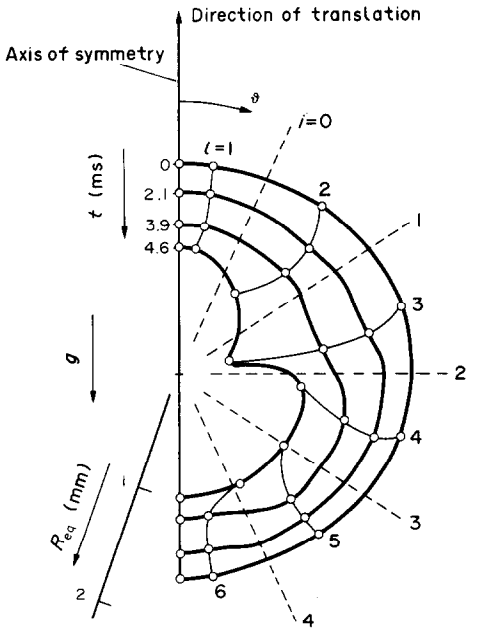

FIG. 8a. Numerically calculated profile of the free translating vapour bubble of Fig. 7a, imploding in a pressure field (cf. Fig. 5) at various instants. $N = 5$, $g = 9.81$ m s^{-2}.

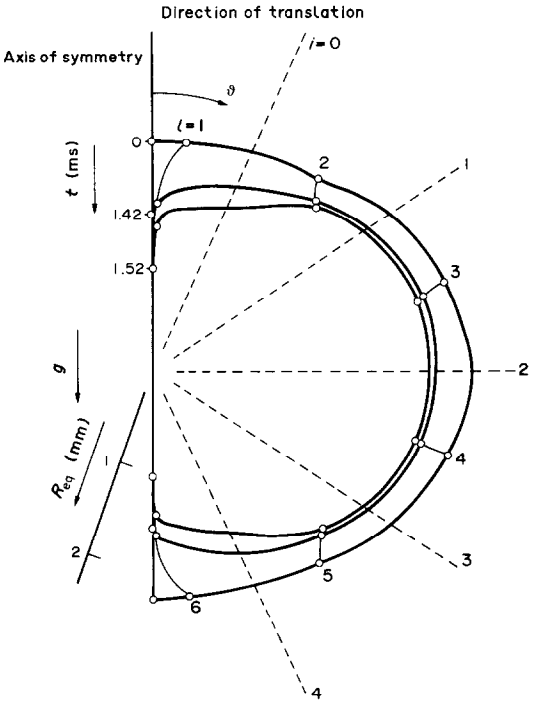

FIG. 8b. Numerically calculated profile of the free translating vapour bubble of Fig. 7b, imploding in a pressure field (cf. Fig. 6) at various instants. $N = 5$, $g = 9.81$ m s^{-2}.

certain conditions. The stability of the bubble shape during implosion depends on the initial conditions, for example, the initial bubble shape and the initial equivalent bubble radius (at equal translational velocities).

In addition to the continuity and momentum equations for the liquid (which are sufficient to describe gas bubble implosion), the energy equation for both the liquid and the vapour must be taken into account in order to describe vapour bubble implosion correctly, see Sections 4.1 and 4.2. Numerical analysis is shown to be able to describe the fragmentation and vapour bubbles, see also ref. [1].

Acknowledgement—The authors are indebted very much to J. G. M. Niessen for his aid in setting up the electronics of the experiments.

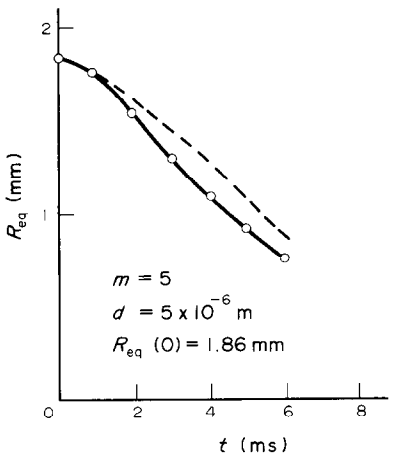

FIG. 9. The experimental and numerically calculated equivalent bubble radius for the bubble of Fig. 7a.

REFERENCES

1. W. M. Sluijter, S. J. D. van Stralen and W. Zijl, The method of characteristics applied to numerical solutions of gas bubble implosion and fragmentation, *Int. J. Heat Mass Transfer* **25,** 1103–1111 (1982).
2. W. Zijl, The hydrodynamics of vapour and gas bubbles by numerical approximations methods. In *Boiling Phenomena* (Edited by S. J. D. van Stralen and R. Cole). Hemisphere, Washington D.C. (1979).
3. W. Zijl, Global collocation approximations of the flow and temperature fields around a gas and vapour bubble, *Int. J. Heat Mass Transfer* **22,** 487–498 (1977).
4. W. Zijl, F. J. M. Ramakers and S. J. D. van Stralen, Global numerical solutions of growth and departure of a vapour bubble at a horizontal superheated wall in a pure liquid and a binary mixture, *Int. J. Heat Mass Transfer* **22,** 401–420 (1979).
5. J. G. H. Joosten, W. Zijl and S. J. D. van Stralen, Growth of a vapour bubble in combined gravitational and non-uniform temperature fields, *Int. J. Heat Mass Transfer* **21,** 15–23 (1978).

6. W. Zijl, Departure of a bubble growing on a horizontal wall. Ph.D. thesis, Eindhoven University of Technology, The Netherlands (1978).
7. L. Fox and I. B. Parker, *Chebychev Polynomials in Numerical Analysis*. Oxford University Press, London (1968).

COMPORTEMENT D'UNE BULLE DE VAPEUR EN TRANSLATION SOUS L'INFLUENCE D'UN SAUT DE PRESSION. SOLUTIONS NUMERIQUES DE L'IMPLOSION ET DE LA FRAGMENTATION

Résumé—L'implosion d'une bulle libre de vapeur, sphérique à l'origine sous l'effet d'un saut de pression est décrite par une solution numérique des équations descriptives. Le traitement est basé sur l'application d'une combinaison des méthodes mathématiques de collocation et des caractéristiques. Le comportement d'une bulle de vapeur est une généralisation du comportement dû à l'effet de la transition de phase, à la paroi de la bulle. Contrairement à une bulle de gaz, une bulle de vapeur diminue complètement pendant l'implosion. Les prévisions théoriques incluent la forme de la bulle et la fragmentation, en accord qualitatif avec de nouveaux résultats expérimentaux.

DAS VERHALTEN EINER SICH BEWEGENDEN DAMPFBLASE UNTER DEM EINFLUSS EINER SPRUNGHAFTEN DRUCKÄNDERUNG: NUMERISCHE LÖSUNGEN FÜR DIE IMPLOSION UND FRAGMENTATION

Zusammenfassung—Mit Hilfe der numerischen Lösung der Grundgleichungen wird die Implosion einer sich bewegenden, ursprünglich kugelförmigen, freien Dampfblase unter dem Einfluß einer sprunghaften Druckänderung beschrieben. Die Behandlung beruht auf einer Kombination des mathematischen Kollokations- und des Charakteristikenverfahrens. Das Verhalten einer Dampfblase ist die Verallgemeinerung des Verhaltens einer Gasblase unter Einbeziehung des Effekts des Phasenübergangs an der Phasengrenzfläche. Im Gegensatz zu einer Gasblase verschwindet die Dampfblase vollständig während der Implosion. Die theoretischen Berechnungen umfassen unter anderem die Blasengestalt und die Fragmentation, die mit neuen experimentellen Ergebnissen gut übereinstimmen.

О ПОВЕДЕНИИ ПЕРЕМЕЩАЮЩЕГОСЯ ПАРОВОГО ПУЗЫРЬКА ПОД ДЕЙСТВИЕМ СКАЧКА ДАВЛЕНИЯ. ЧИСЛЕННЫЕ РЕШЕНИЯ ЗАДАЧ О ВЗРЫВЕ И ДРОБЛЕНИИ

Аннотация—На основании уравнений переноса численно решена задача о взрыве перемещающегося, изначально сферического, свободного пузырька пара под действием скачка давления. Рассмотрение основано на применении комбинации методов коллокации и характеристик. Поведение парового пузырька представляет собой обобщение динамики пузырька газа с учетом эффекта фазового перехода на стенке пузырька. В отличие от пузырька газа паровой пузырек в процессе внутреннего взрыва уменьшается. Теоретические расчеты формы пузырька и дробления находятся в качественном соответствии с экспериментальными данными.